PCCP

Enhanced electrochemical hydrogen oxidation reaction and suppressed hydrogen peroxide generation properties on Pt/Ir(111) bimetallic surfaces

Journal:	*Physical Chemistry Chemical Physics*
Manuscript ID	CP-COM-11-2022-005430
Article Type:	Communication
Date Submitted by the Author:	20-Nov-2022

Complete List of Authors:	Hayashi, Kenta; Tohoku Daigaku, Graduate School of Environmental Studies Tomimori, Takeru; Tohoku Daigaku, Graduate School of Environmental Studies Sato, Riku; Tohoku Daigaku, Graduate School of Environmental Studies Todoroki, Naoto; Tohoku University, Graduate School of Environmental Studies Wadayama, Toshimasa; Tohoku University, Graduate School of Environmental Studies

PCCP

COMMUNICATION

Enhanced electrochemical hydrogen oxidation reaction and suppressed hydrogen peroxide generation properties on Pt/Ir(111) bimetallic surfaces

Received 00th XX 20xx,
Accepted 00th XX 20xx

DOI: 10.1039/x0xx00000x

Kenta Hayashi,*[a] Takeru Tomimori,[a] Riku Sato,[a] Naoto Todoroki,[a] and Toshimasa Wadayama[a]

Simultaneous accomplishment of high hydrogen oxidation reaction (HOR) activity and suppressed hydrogen peroxide (H_2O_2) generation is desired for anode catalysts of polymer electrolyte fuel cells. 0.3 monolayer-thick-Pt-deposited Ir(111) showed threefold higher HOR activity than Pt(111) and suppressed H_2O_2 generation under the detection limit, providing insight for the effective catalyst development.

Polymer electrolyte fuel cells (PEFCs) are attracting attention as a promising clean energy source for automotive and static applications. Despite the significant effort made to date for its widespread use, the high cost and short lifetime of PEFCs remain unresolved. In terms of lifetime, the degradation of materials used for PEFCs needs to be prevented. Chemical degradation of the proton exchange membrane (PEM) is one of the representative targets.[1] This degradation scenario is considered as follows: first, the crossover O_2 from the cathode is reduced on the anode catalyst,[2] which originally aims to promote the hydrogen oxidation reaction (HOR). Presently, carbon-supported Pt nanoparticles (Pt/C) are used as PEFC anode catalysts, and it is known that the oxygen reduction reaction (ORR) on Pt/C accompanies a 2-electron pathway in the anode potential region (close to 0 V *vs*. RHE), resulting in hydrogen peroxide (H_2O_2) generation.[3] Thereafter, H_2O_2 decomposes into reactive oxygen-related radicals (•OH), which attack and degrade the PEM.[4] Therefore, the development of a novel anode catalyst having characteristics of suppressed H_2O_2 generation and sufficient HOR activity is desired.[5–7]

Fundamental investigation using well-defined surfaces of single crystals is one of the powerful methods for investigating effective catalyst materials. This is because the surface structure of practical supported nanoparticle catalysts, especially alloy nanoparticle catalysts, are highly complex, e.g., inhomogeneous topmost surface composition, atomic arrangement, etc., making it difficult to distinguish the well-acknowledged factors influencing catalytic properties such as the bifunctional (ensemble) effect, ligand effect, and strain effect.[8–10]

In this study, the aforementioned catalyst properties for Pt–Ir bimetallic surfaces are fundamentally investigated. Pt–Ir bimetallic materials have been investigated as fascinating electrocatalysts for such as PEFC cathode,[11–13] unitized regenerative fuel cell anode,[14] direct ammonia fuel cell anode,[15,16] direct methanol fuel cell anode,[17] etc., yet have not been investigated as less-H_2O_2-generating PEFC anode. Recently, we showed that the Ir surface can provide the appropriate catalytic properties for PEFC anode by investigating both H_2O_2 generation and HOR properties for low-index single crystal surfaces of Ir (Ir(*hkl*), *hkl* = 111, 100, and 110): Ir(111) exhibited suppressed H_2O_2 generation (below the detection limit) and relatively high HOR activity (ca. 70% of Pt(111)),[18] which suggests that Ir addition to PEFC anode catalysts might be effective. In this work, we fabricated a well-defined model of bimetallic surface structures on Ir(111) single crystal substrate with different surface coverages of Pt (Pt_{xML}/Ir(111)) and investigated the HOR and H_2O_2 generation properties in acidic media using tip generation/substrate collection (TG/SC)[19–21] and substrate generation/tip collection (SG/TC)[22,23] modes of scanning electrochemical microscope (SECM), respectively. We focused on the bimetallic surface models with submonolayer Pt coverage rather than those with fully Pt-covered surfaces. The experimental results indicate that the Ir(111) surface covered with appropriate amounts of Pt submonolayers ($Pt_{0.3ML}$/Ir(111)) exhibits enhanced HOR activity and suppressed H_2O_2

[a] *Graduate School of Environmental Studies, Tohoku University, Sendai 980-8579, JAPAN*

Electronic Supplementary Information (ESI) available: (A) Detailed explanation for estimation of Pt coverage from XPS, (B) XP spectra before and after annealing, (C) Low energy electron diffraction (LEED) patterns, (D) Scanning tunneling microscope (STM) observation, (E) Experimental procedure for SECM measurements and the detailed results of (1) HOR activity and (2) H_2O_2 generation property evaluation, (F) Cyclic voltammograms (CVs). See DOI: 10.1039/x0xx00000x

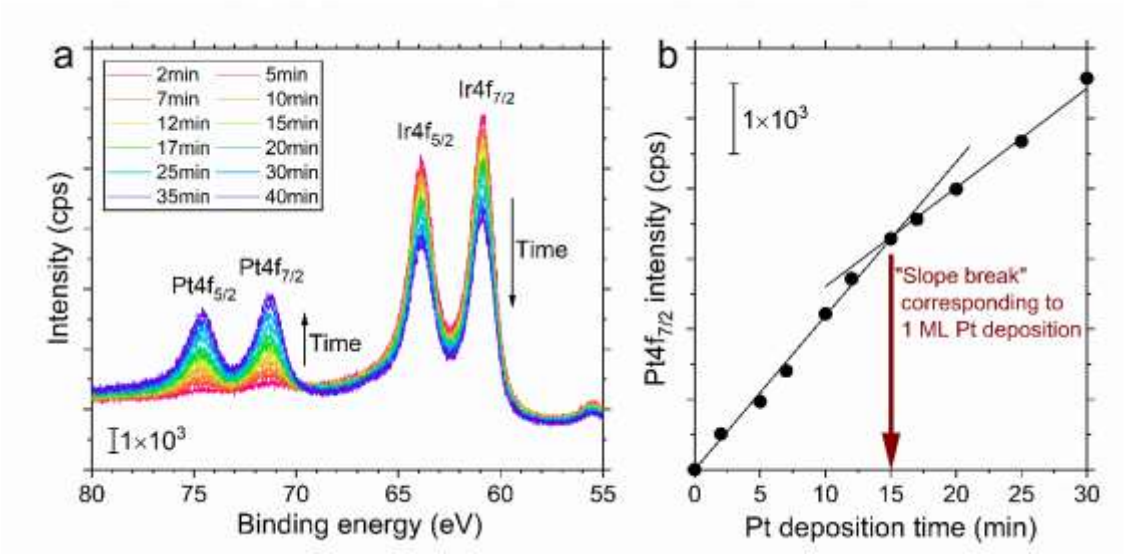

Figure 1. XP spectra measured with increasing Pt deposition time on an Ir(111) substrate surface. (a) Spectra in Pt4f and Ir4f region. (b) Plot of the $Pt4f_{7/2}$ band intensity against the deposition time.

generation. The modified hydrogen adsorption on the bimetallic surfaces can be proposed as the HOR activity enhancement factors, while H_2O_2-related intermediate reduction at Ir sites (bifunctional effect) can be suggested as a possible factor of suppressed H_2O_2 generation.

Model catalyst surfaces were prepared in an ultrahigh-vacuum (UHV) system. The surface of the single crystal Ir(111) substrate was cleaned by repeated cycles of Ar^+ sputtering and annealing at 1183 K in UHV. Thereafter, *x* monolayer-thick (*x* = 0.1, 0.3, and 0.5 monolayer (ML)) of Pt was deposited on the cleaned Ir(111) using electron-beam evaporation method.[24] During the depositions, the substrate temperature remained constant at room temperature We quantified the Pt coverage based on X-ray photoelectron spectroscopy (XPS) measurements, in which Pt was continuously deposited on Ir(111) and the Pt and Ir 4f bands were measured (Figure 1 (a)). As shown in Figure 1 (b), the $Pt4f_{7/2}$ intensity increases linearly with increasing Pt deposition time until the "slope-break" is reached at about 15 min, corresponding to one monolayer-thick Pt.[25,26] A more detailed explanation and spectral fitting results are shown in ESI. A. This estimation was in good agreement with the deposition rate measured using a quartz crystal oscillator installed in the UHV chamber (approximately 0.2 $Å_{Pt}$/min); hence, based on the results, the deposition amount of Pt for each experiment was checked and calibrated using the oscillator. During this XPS measurement, we checked the binding energies of Pt 4f bands. The values shifted to a higher binding energy side compared with those for pure Pt^0–(Figure S.1 (a)). Thereafter, the Pt-deposited Ir(111) substrates were annealed at 673 K for 30 min. Note that the Pt4f spectra remained unchanged by the UHV-annealing, as shown in ESI.B. The low energy electron diffraction (LEED) patterns of the as-fabricated samples are shown in Figure S.3 (ESI. C), in which 6-fold surface symmetry was basically confirmed, though the diffraction spots tend to be diffuse with increasing Pt thicknesses of *x*. We also performed scanning tunneling microscopy (STM) for the $Pt_{0.3ML}$/Ir(111) surface (Figure S.2 in ESI. D), which demonstrated the best catalytic performance in this study (shown in a later section), where the bimetallic surface of epitaxial Pt islands and Ir(111) terraces can be observed.

The prepared Pt/Ir(111) samples were transferred from the UHV chamber to the SECM system without exposing the sample surface to air using a homebuilt transfer system.[18,27] Contrary to the conventional rotating disk electrode (RDE) method, which is pointed out to underestimate the quite fast reaction rate of HOR

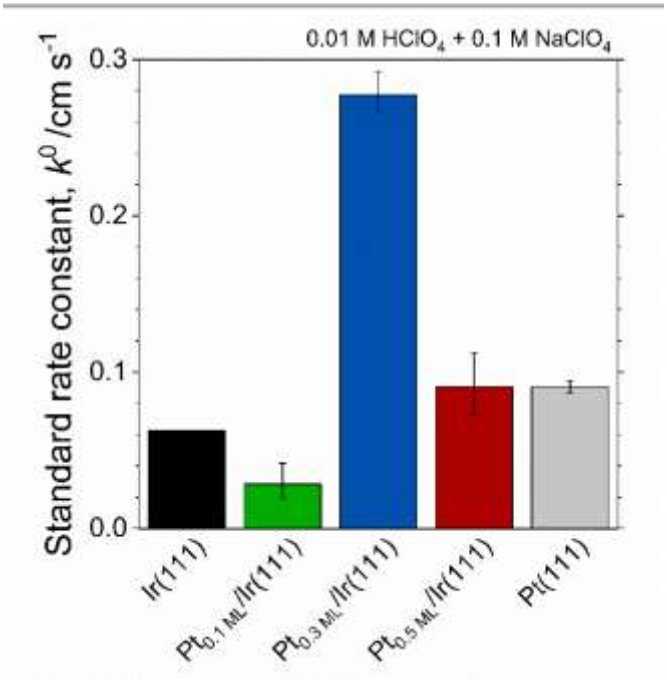

Figure 2. HOR standard rate constants (k^0) for Pt_{xML}/Ir(111) estimated by TG/SC mode of SECM.

in acidic solutions, SECM can quantify the standard rate constant of HOR.[20,28] Furthermore, SECM is capable of evaluating H_2O_2 generation during ORR.[29,30] Therefore, in this communication, we adopt SECM to evaluate HOR and H_2O_2 generation properties of Pt_{xML}/Ir(111) model anode catalyst surfaces. A detailed experimental procedure of the SECM measurements is described in ESI. E and our previous research.[18] In addition, cyclic voltammograms (CVs) of Pt_{xML}/Ir(111) recorded in N_2-purged 0.1 M $HClO_4$ by using a conventional three electrode cell are displayed in Figure S.6 in ESI. F, in which detailed conditions of the CV measurements are also described.

Figure 2 shows the estimated k^0-values for HOR, i.e., HOR activity, evaluated in 0.01 M $HClO_4$ + 0.1 M $NaClO_4$ using the tip generation/substrate collection (TG/SC) mode of SECM. The experimental data and the fitting results used to estimate k^0-values are shown in ESI. E (Figure S.5). The k^0-values of vacuum-cleaned Ir(111) and Pt(111) from our recent literature[18] are also displayed as references in Figure 2. As for the submonolayer-thick-Pt-deposited samples (x = 0.1, 0.3, and 0.5), $Pt_{0.3ML}$/Ir(111) (blue) and $Pt_{0.5ML}$/Ir(111) (red) outperformed Ir(111) (black). Especially, the HOR activity of $Pt_{0.3ML}$/Ir(111) (blue) was threefold higher than that of clean Pt(111) (gray). In contrast, the estimated HOR activity of $Pt_{0.1ML}$/Ir(111) (green) was even lower than that of Ir(111). The results indicate that the HOR activity of the bimetallic surface with (111) surface atomic arrangement strongly depends on the surface atomic ratio of Ir : Pt, with the ratio of Ir : Pt = 7 : 3 concluded as the most appropriate for enhancing the HOR activity. This result obtained for the well-defined Pt_{xML}/Ir(111) corresponds well with the previous study for the bulk Pt-Ir alloys, which concluded that the sample with bulk atomic ratio of Pt : Ir = 3 : 7 most effectively catalyzes HOR.[21]

The HOR activity enhancement would be dominated by dissociations and adsorption of H_2 on bimetallic surfaces that modified by both electronic and structural factors. To date, the two possible mechanisms are suggested for HOR in acidic solution: Tafel-Volmer or Heyrovsky-Volmer mechanisms, composed of the reaction steps such as Tafel step ($H_2 \rightarrow 2H_{ad}$), Heyrovsky step ($H_2 \rightarrow H_{ad} + H^+ + e^-$), and Volmer step ($H_{ad} \rightarrow H^+ + e^-$). For both mechanisms, binding energy of adsorbed hydrogen (H_{ad}) is important factor of HOR activity. Because the bonding of H_{ad} to the Pt and Ir surfaces is considered to be stronger compared with that for optimal HOR activity enhancement,[31,32] appropriately weakened H_{ad} bonding would show maximum HOR activity for Pt_{xML}/Ir(111). According to the literatures, the coexistence of Pt and Ir can result in interatomic charge transfer,[13,33] and this is consistent with the chemical shift of Pt4f observed in the present study (Figure S.2) though the shift of Ir4f was difficult to discuss due to the strong photoelectron intensity from Ir(111) substrate (Figure S.1 (b)). Besides, the upshift and downshift of the *d*-band centers can be expected for Ir and Pt in Pt_{xML}/Ir(111), respectively, based on the theoretical calculation by Ruban et al.[34] Since the upshift of the d-band center tends to strengthen the hydrogen binding,[35,36] hydrogen binding strength of surface Pt and Ir domains can be expected to become lower and higher, respectively. From this perspective, deposited Pt sites rather than substrate Ir sites are more likely to contribute to the HOR activity enhancement for Pt_{xML}/Ir(111). Despite possible electronic factors for the HOR activity enhancement, such as *d*-band center of Pt_{xML}/Ir(111), the obtained HOR activity trend against the deposited amounts of Pt deviated from so-called a volcano shape (Figure 2). Such experimental result implies the factors other than the electronic factors of Pt_{xML}/Ir(111) might dominate HOR activity. The most likely factor is the surface morphology of Pt_{xML}/Ir(111), where various sizes of Pt islands (approximately 10 nm wide and monoatomic height) are dispersed on Ir(111) terraces (Figure S.4 ESI. D). The number of interfacial sites of the Pt-islands and Ir(111) terraces and/or hydrogen spill over[37] between Pt and Ir adjacent sites should depend on the surface morphology, thereby correlate with HOR of Pt_{xML}/Ir(111).

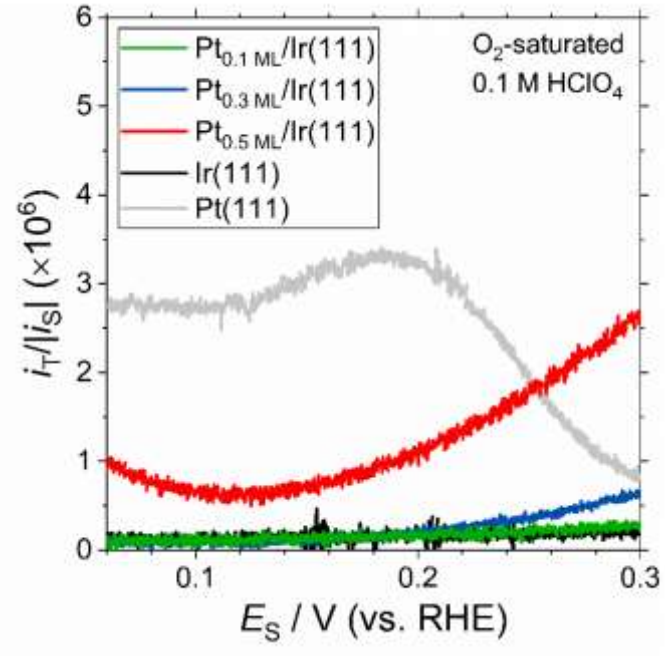

Figure 3. H_2O_2 generation properties of the Pt_{xML}/Ir(111) evaluated by the SG/TC mode of SECM.

The results of substrate generation/tip collection (SG/TC) measurement for H_2O_2 generation properties are summarized in Figure 3. The sample potential (E_S)-dependence of H_2O_2 detection current (i_T) normalized by sample electrode current originating from ORR ($|i_S|$) was displayed from the

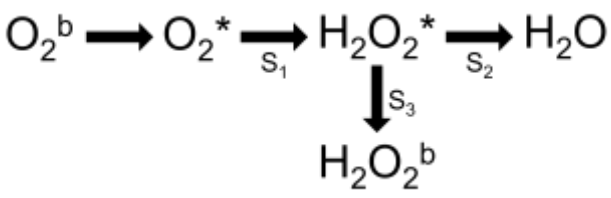

Scheme 1. Simplified model for ORR process. Superscripts * and b denote the intermediate species on the electrode surface and the species in the bulk solution, respectively.

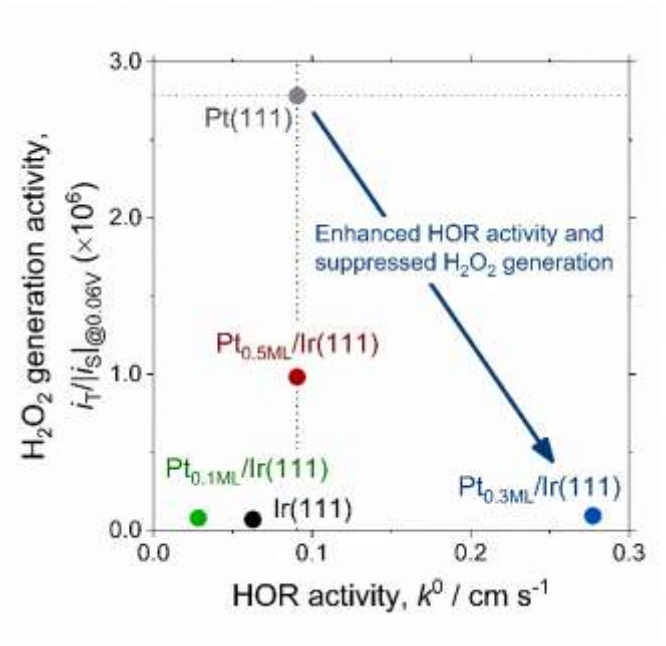

Figure 4. Summary of the H_2O_2 generation and HOR properties for Pt_{xML}/Ir(111), in comparison with vacuum-cleaned Ir(111) and Pt(111).[18]

measurements in O_2-saturated 0.1 M $HClO_4$. The data for vacuum-cleaned Pt(111) and Ir(111) collected in our previous study[18] are shown as references. The experimental data for i_T and i_S are shown in ESI. E (Figure S.6). Figure 3 indicates that the $i_T/|i_S|$-value for $Pt_{0.1ML}$/Ir(111) (green) is a noise level throughout the potential range (0.06 V < E_S < 0.3 V) similar to clean Ir(111). Also, the value of $i_T/|i_S|$ for $Pt_{0.3ML}$/Ir(111) (blue) remained almost at the noise level below 0.2 V, though $i_T/|i_S|$ slightly increased in E_S > 0.2 V. In contrast, the value of $i_T/|i_S|$ for $Pt_{0.5ML}$/Ir(111) (red) exhibited marked H_2O_2 generation throughout the potential range of 0.06–0.3 V. The results indicate that the value of x (Pt-deposited thicknesses) less than 0.5 ML for Pt_{xML}/Ir(111) tends to suppress the H_2O_2 generation in the potential region of <0.2 V, which seems consistent with several studies reporting for H_2O_2 generation through ORR on the Pt–Ir catalysts with Pt-enriched surfaces.[33,38,39] The present study revealed that the Ir-enriched surfaces of Ir-Pt bimetallic materials, contrary to the Pt-enriched surfaces, are effective in mitigating the H_2O_2 generation.

The suppressed H_2O_2 generation properties of $Pt_{0.1ML}$/Ir(111) and $Pt_{0.3ML}$/Ir(111) can be explained through facilitated H_2O_2 reduction to H_2O at Ir sites, i.e., bifunctional mechanism.[40] Scheme 1 is the simplified model for multistep ORR process.[41] In this model, the kinetic parameters of the sub-processes S_1 (intermediate H_2O_2 formation), S_2 (H_2O_2 reduction to H_2O), and S_3 (H_2O_2 desorption and diffusion into bulk solution) determine the H_2O_2 generation behavior. The generation of large amounts of H_2O_2 on clean Pt(111) is considered as the consequence of the prohibited H_2O_2 reduction (S_2 in scheme 1) in the relatively low potential (approximately < 0.3 V).[42] Meanwhile, Ir sites could reduce the intermediate H_2O_2 to H_2O because clean Ir(111) hardly generates H_2O_2 during ORR in this potential region. Thus, even if H_2O_2 was generated at adjacent Pt sites, it could be reduced to H_2O on Ir sites before its desorption into bulk solution, resulting in suppressed H_2O_2 generations for Pt_{xML}/Ir(111) surfaces.

Figure 4 summarizes the HOR and H_2O_2 generation properties of the investigated Pt_{xML}/Ir(111), displaying k^0-values estimated by TG/SC measurements (Figure 2) on the x-axis and $i_T/|i_S|$-values at 0.06 V obtained by SG/TC measurements (Figure 3) on the y-axis as representative values of HOR and H_2O_2 generation properties, respectively. The summarized results clearly show that the coexistence of Ir and Pt surface sites with a Pt/Ir ratio of approximately 3 : 7 ($Pt_{0.3ML}$/Ir(111)) can achieve both high HOR activity and suppressed H_2O_2 generation that outperformed clean Pt(111), which are desirable properties as the novel PEFC anode catalyst mitigating the PEM degradation. The factors of high HOR activity and suppressed H_2O_2 generation would result from the modified hydrogen adsorption on Pt/Ir(111) bimetallic surfaces and facilitated H_2O_2 reduction on adjacent Ir sites, respectively.

Conclusions

Submonolayer-thick-Pt-deposited Ir(111) (Pt_{xML}/Ir(111); x = 0.1, 0.3, 0.5) was fabricated as well-defined model catalysts to investigate the two fundamental electrochemical reactions related to PEFC anode: HOR and H_2O_2 generation in acidic media. $Pt_{0.3ML}$/Ir(111), especially, showed desirable performances: the simultaneous accomplishment of enhanced HOR activity (threefold higher standard rate constant than Pt(111)) and suppressed H_2O_2 generation (below the detection limit at the potential region close to 0 V *vs*. RHE), which are discussed based on the modification of hydrogen adsorption and bifunctional mechanism of the UHV-fabricated Pt–Ir bimetallic surfaces, respectively.

Author Contributions

KH was involved in the investigation, visualization, writing of original draft, and editing. TT and RS were involved in the investigation. NT was involved in review and editing. TW was involved in conceptualization, funding acquisition, project administration, supervision, and review and editing. All authors have approved the final version of the manuscript.

Conflicts of interest

There are no conflicts to declare.

Acknowledgement

This study was supported by JSPS KAKENHI Grant Number JP21H01645 (TW), JST SPRING Grant Number JPMJSP2114 (KH), and the New Energy and Industrial Technology Development Organization (NEDO) of Japan.

References

1 R. Borup, J. Meyers, B. Pivovar, Y. S. Kim, R. Mukundan, N. Garland, D. Myers, M. Wilson, F. Garzon, D. Wood, P. Zelenay, K. More, K. Stroh, T. Zawodzinski, J. Boncella, J. E. McGrath, M. Inaba, K. Miyatake, M. Hori, K. Ota, Z. Ogumi, S. Miyata, A. Nishikata, Z. Siroma, Y. Uchimoto, K. Yasuda, K. Kimijima and N. Iwashita, Scientific Aspects of Polymer Electrolyte Fuel Cell Durability and Degradation, *Chem. Rev.*, 2007, **107**, 3904–3951.

2 M. Inaba, T. Kinumoto, M. Kiriake, R. Umebayashi, A. Tasaka and Z. Ogumi, Gas crossover and membrane degradation in polymer electrolyte fuel cells, *Electrochim. Acta*, 2006, **51**, 5746–5753.

3 O. Antoine and R. Durand, RRDE study of oxygen reduction on Pt nanoparticles inside Nafion: H2O2 production in PEMFC cathode conditions, *J. Appl. Electrochem.*, 2000, **30**, 839–844.

4 Q. Tang, B. Li, D. Yang, P. Ming, C. Zhang and Y. Wang, Review of hydrogen crossover through the polymer electrolyte membrane, *Int. J. Hydrogen Energy*, 2021, **46**, 22040–22061.

5 G. Shi, D. A. Tryk, T. Iwataki, H. Yano, M. Uchida, A. Iiyama and H. Uchida, Unparalleled mitigation of membrane degradation in fuel cells via a counter-intuitive approach: Suppression of H2O2 production at the hydrogen anode using a Ptskin-PtCo catalyst, *J. Mater. Chem. A*, 2020, **8**, 1091–1094.

6 H. Uchida, G. Shi, M. Imran and D. A. Tryk, Particle-Size Effect of Pt Anode Catalysts on H2O2 Production Rate and H2 Oxidation Activity at 20 to 80 °C, *J. Electrochem. Soc.*, 2022, **169**, 014516.

7 Y. Nakamori, N. Suzuki, K. Tanaka, T. Aoki, T. Nohira and R. Hagiwara, Pt–Ru Anode Catalyst to Suppress H2O2 Formation due to Oxygen Crossover, *J. Electrochem. Soc.*, 2018, **165**, F463–F467.

8 Z. Xia and S. Guo, Strain engineering of metal-based nanomaterials for energy electrocatalysis, *Chem. Soc. Rev.*, 2019, **48**, 3265–3278.

9 C. A. Angelucci, J. Souza-Garcia and J. M. Feliu, The role of adsorbates in electrocatalytic systems: An analysis of model systems with single crystals, *Curr. Opin. Electrochem.*, 2021, **26**, 100666.

10 Z. Ma, Z. P. Cano, A. Yu, Z. Chen, G. Jiang, X. Fu, L. Yang, T. Wu, Z. Bai and J. Lu, Enhancing Oxygen Reduction Activity of Pt-based Electrocatalysts: From Theoretical Mechanisms to Practical Methods, *Angew. Chemie*, 2020, **132**, 18490–18504.

11 J. Zhu, A. O. Elnabawy, Z. Lyu, M. Xie, E. A. Murray, Z. Chen, W. Jin, M. Mavrikakis and Y. Xia, Facet-controlled Pt–Ir nanocrystals with substantially enhanced activity and durability towards oxygen reduction, *Mater. Today*, 2020, **35**, 69–77.

12 J. Bak, H. Kim, S. J. Lee, M. J. Kim, E. J. Kim, J. H. Roh, J. W. Shin, C. H. Choi and E. A. Cho, Boosting the Role of Ir in Mitigating Corrosion of Carbon Support by Alloying with Pt, *ACS Catal.*, 2020, **10**, 12300–12309.

13 T. Ioroi and K. Yasuda, Platinum-Iridium Alloys as Oxygen Reduction Electrocatalysts for Polymer Electrolyte Fuel Cells, *J. Electrochem. Soc.*, 2005, **152**, A1917–A1924.

14 P. Kúš, A. Ostroverkh, I. Khalakhan, R. Fiala, Y. Kosto, B. Šmíd, Y. Lobko, Y. Yakovlev, J. Nováková, I. Matolínová and V. Matolín, Magnetron sputtered thin-film vertically segmented Pt-Ir catalyst supported on TiC for anode side of proton exchange membrane unitized regenerative fuel cells, *Int. J. Hydrogen Energy*, 2019, **44**, 16087–16098.

15 R. Chen, S. Zheng, Y. Yao, Z. Lin, W. Ouyang, L. Zhuo and Z. Wang, Performance of direct ammonia fuel cell with PtIr/C, PtRu/C, and Pt/C as anode electrocatalysts under mild conditions, *Int. J. Hydrogen Energy*, 2021, **46**, 27749–27757.

16 N. Sacré, M. Duca, S. Garbarino, R. Imbeault, A. Wang, A. Hadj Youssef, J. Galipaud, G. Hufnagel, A. Ruediger, L. Roué and D. Guay, Tuning Pt-Ir Interactions for NH3 Electrocatalysis, *ACS Catal.*, 2018, **8**, 2508–2518.

17 E. N. El Sawy and V. I. Birss, Nanoengineered Ircore@Ptshell Nanoparticles with Controlled Pt Shell Coverages for Direct Methanol Electro-Oxidation, *ACS Appl. Mater. Interfaces*, 2018, **10**, 3459–3469.

18 K. Hayashi, T. Tomimori, Y. Chida, N. Todoroki and T. Wadayama, Hydrogen Peroxide Generation and Hydrogen Oxidation Reaction Properties of Ir(111)-, (100)-, and (110)-Low-Index Single-Crystal Surfaces, *J. Phys. Chem. C*, 2021, **125**, 21481–21487.

19 J. Zhou, Y. Zu and A. J. Bard, Scanning electrochemical microscopy - Part 39. The proton/hydrogen mediator system and its application to the study of the electrocatalysis of hydrogen oxidation, *J. Electroanal. Chem.*, 2000, **491**, 22–29.

20 C. G. Zoski, Scanning electrochemical microscopy: Investigation of hydrogen oxidation at polycrystalline noble metal electrodes, *J. Phys. Chem. B*, 2003, **107**, 6401–6405.

21 Y. C. Weng and C. T. Hsieh, Scanning electrochemical microscopy characterization of bimetallic Pt–M (M=Pd, Ru, Ir) catalysts for hydrogen oxidation, *Electrochim. Acta*, 2011, **56**, 1932–1940.

22 C. M. Sánchez-Sánchez, J. Rodríguez-López and A. J. Bard, Scanning electrochemical microscopy. 60. Quantitative calibration of the SECM substrate generation/tip collection mode and its use for the study of the oxygen reduction mechanism, *Anal. Chem.*, 2008, **80**, 3254–3260.

23 A. Kishi, S. Shironita and M. Umeda, H2O2 detection analysis of oxygen reduction reaction on cathode and anode catalysts for polymer electrolyte fuel cells, *J. Power Sources*, 2012, **197**, 88–92.

24 N. Todoroki, H. Watanabe, T. Kondo, S. Kaneko and T. Wadayama, Highly Enhanced Oxygen Reduction Reaction Activity and Electrochemical Stability of Pt/Ir(111) Bimetallic Surfaces, *Electrochim. Acta*, 2016, **222**, 1616–1621.

25 X. F. Yang, W. Xu, M. Li, B. E. Koel and J. G. Chen, A new class of electrocatalysts of supporting Pt on an Engel-Brewer alloy substrate: A demonstration for oxidation of ethylene glycol, *Chem. Commun.*, 2014, **50**, 12981–12984.

26 H. Siegfried, *Auger- and X-Ray Photoelectron Spectroscopy in Materials Science*, Springer, 2013.

27 T. Wadayama, N. Todoroki, Y. Yamada, T. Sugawara, K. Miyamoto and Y. Iijama, Oxygen reduction reaction activities of Ni/Pt(111) model catalysts fabricated by molecular beam epitaxy, *Electrochem. commun.*, 2010, **12**, 1112–1115.

28 J. Durst, C. Simon, F. Hasché and H. A. Gasteiger, Hydrogen Oxidation and Evolution Reaction Kinetics on Carbon Supported Pt, Ir, Rh, and Pd Electrocatalysts in Acidic Media, *J. Electrochem. Soc.*, 2015, **162**, F190–F203.

29 Y. Shen, M. Träuble and G. Wittstock, Detection of hydrogen peroxide produced during electrochemical oxygen reduction using scanning electrochemical microscopy, *Anal. Chem.*, 2008, **80**, 750–759.

30 C. M. Sánchez-Sánchez and A. J. Bard, Hydrogen peroxide production in the oxygen reduction reaction at different electrocatalysts as quantified by scanning electrochemical microscopy, *Anal. Chem.*, 2009, **81**, 8094–8100.

31 M. P. Mercer and H. E. Hoster, Electrochemical Kinetics: a Surface Science-Supported Picture of Hydrogen Electrochemistry on Ru(0001) and Pt/Ru(0001), *Electrocatalysis*, 2017, **8**, 518–529.

32 J. Zheng, Z. Zhuang, B. Xu and Y. Yan, Correlating Hydrogen Oxidation/Evolution Reaction Activity with the Minority Weak Hydrogen-Binding Sites on Ir/C Catalysts, *ACS Catal.*, 2015, **5**, 4449–4455.

33 N. Bhuvanendran, S. Ravichandran, S. S. Jayaseelan, Q. Xu, L. Khotseng and H. Su, Improved bi-functional oxygen electrocatalytic performance of Pt–Ir alloy nanoparticles embedded on MWCNT with Pt-enriched surfaces, *Energy*, 2020, **211**, 118695.

34 A. Ruban, B. Hammer, P. Stoltze, H. L. Skriver and J. K. Nørskov, Surface electronic structure and reactivity of transition and noble metals, *J. Mol. Catal. A Chem.*, 1997, **115**, 421–429.

35 J. R. De Lile, A. Bahadoran, Q. Liu, S. Woo Lee, C. Pak, J. Zhang and S. G. Lee, First principles study of Ir3Ru, IrRu and IrRu3 catalysts for hydrogen oxidation reaction: Effect of surface modification and ruthenium content, *Appl. Surf. Sci.*, 2021, **545**, 149002.

36 J. Greeley, J. K. Nørskov, L. A. Kibler, A. M. El-Aziz and D. M. Kolb, Hydrogen evolution over bimetallic systems: Understanding the trends, *ChemPhysChem*, 2006, **7**, 1032–1035.

37 H. Hoster, B. Richter and R. J. Behm, Catalytic influence of Pt monolayer islands on the hydrogen electrochemistry of Ru(0001) studied by ultrahigh vacuum scanning tunneling microscopy and cyclic voltammetry, *J. Phys. Chem. B*, 2004, **108**, 14780–14788.

38 J. Zhang, M. B. Vukmirovic, Y. Xu, M. Mavrikakis and R. R. Adzic, Controlling the catalytic activity of platinum-monolayer electrocatalysts for oxygen reduction with different substrates, *Angew. Chemie - Int. Ed.*, 2005, **44**, 2132–2135.

39 A. U. Nilekar, Y. Xu, J. Zhang, M. B. Vukmirovic, K. Sasaki, R. R. Adzic and M. Mavrikakis, Bimetallic and ternary alloys for improved oxygen reduction catalysis, *Top. Catal.*, 2007, **46**, 276–284.

40 K. Hayashi, K. Kusunoki, T. Tomimori, R. Sato, N. Todoroki and T. Wadayama, Hydrogen peroxide generation and hydrogen oxidation reactions of vacuum-prepared Ru/Ir(111) bimetallic surfaces, *Phys. Chem. Chem. Phys.*, 2022, **24**, 14277–14283.

41 F. Yin, Y. Liu, S. Wang, C. Wang and H. Liu, Validation of H2O2-mediated pathway model for elucidating oxygen reduction mechanism: Experimental evidences and theoretical simulations, *Electrochim. Acta*, 2019, **313**, 378–388.

42 V. Briega-Martos, E. Herrero and J. M. Feliu, The inhibition of hydrogen peroxide reduction at low potentials on Pt(111): Hydrogen adsorption or interfacial charge?, *Electrochem. commun.*, 2017, **85**, 32–35.